Laser beam cleanup using improved model-based wavefront sensorless adaptive optics

Bing Dong (董 冰)* and Rui Wang (王 瑞)

School of Optoelectronics, Beijing Institute of Technology, Beijing 100081, China
**Corresponding author: bdong@bit.edu.cn*

Received October 21, 2015; accepted January 8, 2016; posted online February 26, 2016

An improved model-based wavefront sensorless adaptive optics algorithm is proposed for laser beam cleanup. Deformable mirror (DM) eigenmodes are used to replace traditional Lukosz modes in order to avoid DM fitting errors. The traditional method is based on a sophisticated calibration process and solving linear equations. In our method, coefficients of DM eigenmodes are estimated by adding bidirectional modal biases into the system and then solving parabolic equations. The calibration process is omitted in our method, which makes it more feasible. From simulation and experimental results, the corrective accuracy of the improved method is higher than the traditional one.

OCIS codes: 140.3300, 220.1080.
doi: 10.3788/COL201614.031406.

High beam quality is required in most laser-related applications. Adaptive optics (AO) has been proven as an effective way to improve the beam quality[1]. In traditional AO, a dedicated wavefront sensor is generally used to measure the wavefront aberration and a conjugated deformable mirror (DM) is driven to make compensation accordingly. However, the performance of traditional AO can be affected by non-common path error and scintillation. In recent years, wavefront sensorless AO (WSAO) based on model-free algorithms like hill climbing, and genetic and stochastic parallel gradient descent (SPGD), are used to improve the beam quality[2–4]. However, the convergence speed of model-free algorithms highly depends on the control channel number and the achievement of a global optimum is not always guaranteed. Model-based WSAO provides a more efficient way to correct wavefront aberrations[5–8]. In model-based WSAO, wavefront aberration is estimated from the deterministic relationship between Zernike or Lukosz mode coefficients and a well-chosen metric function. The convergence speed of model-based WSAO is much faster than model-free WSAO. Only two or three correction cycles are needed by model-based WSAO, in contrast with several hundreds of iterations typically needed by model-free algorithms.

Although it has been successfully demonstrated in principle, model-based WSAO has drawbacks in practice. In this Letter, a traditional model-based WSAO algorithm is briefly reviewed first, then an improved algorithm is proposed to enhance robustness and accuracy. The superiority of our algorithm is demonstrated both by simulation and experiment.

Phase aberration can be expressed by a linear combination of Lukosz modes[6],

$$\varphi = \sum_{i=4}^{N} a_i L_i = \mathbf{a} \cdot \mathbf{L}, \tag{1}$$

where a_i is the Lukosz mode coefficient, L_i is the Lukosz mode except piston and tip/tilt, and $\mathbf{a}$ and $\mathbf{L}$ are the corresponding vectors.

Unlike Zernike modes, the orthogonality of Lukosz modes is described as

$$\int_0^{2\pi}\int_0^1 \nabla L_j \cdot \nabla L_{j'} r \mathrm{d}r\mathrm{d}\theta = \pi\delta_{jj'}, \tag{2}$$

where ∇ is the gradient operator and $\delta_{jj'}$ is the Kronecker delta.

In the geometrical optics regime, the mean-square radius of the far-field spot is proportional to an integral over the pupil area as[7]

$$\langle\rho^2\rangle \propto \iint_P |\nabla\varphi|^2 \mathrm{d}A. \tag{3}$$

From Eqs. (1) and (2), the integral can be rewritten as

$$\iint_P |\nabla\varphi|^2 \mathrm{d}A = \pi\sum_{i=4}^{N} a_i^2. \tag{4}$$

From Eqs. (3) and (4), the mean-square spot radius $\langle\rho^2\rangle$ is dependent on the modulus square of the Lukosz coefficients,

$$\langle\rho^2\rangle = \mu|\mathbf{a}|^2, \tag{5}$$

where μ is a constant related to optical system parameters.

The metric function J with maximum value 1 is defined as

$$J = \int_\rho\int_\theta I(\rho,\theta)(1-\rho^2/R^2)\rho\mathrm{d}\rho\mathrm{d}\theta = 1 - \frac{\mu}{R^2}|\mathbf{a}|^2, \tag{6}$$

where $I(\rho,\theta)$ is the normalized intensity distribution at the focal-plane detector and R is the detector radius.

In previous works, the coefficient vector **a** is estimated by Eq. (7) based on the approximated linear relationship between **W** and **a**[5,6],

$$\hat{\mathbf{a}} \approx \mathbf{T}^{-1}(\mathbf{W} - \mathbf{W_0}), \tag{7}$$

$$\mathbf{W} = \frac{\sum_{m=1}^{N+1} \mathbf{b}_m J(\mathbf{a} - \mathbf{b}_m)}{\sum_{m=1}^{N+1} J(\mathbf{a} - \mathbf{b}_m)},$$

where **b** is the coefficient vector of the Lukosz mode bias. $\mathbf{W_0}$ is equal to **W** when the input error vector $\mathbf{a} = 0$. Matrix **T** should be calibrated precisely before correction. The elements of matrix **T** are calculated by $T_{ik} = \frac{\partial W_i}{\partial a_k}\big|_{\mathbf{a}=0}$, which indicates that the initial input error should be totally removed before calibration.

The model-based WSAO algorithm narrated above is effective in principle but has some limitations in real applications. First, analytical Lukosz modes can only be approximately generated by a DM in practice. The DM fitting errors will degrade the corrective accuracy especially for low-order AO systems. Simulation and experimental results show that DM eigenmodes are preferable to Lukosz modes since they can be reproduced perfectly by the DM[9–11]. DM eigenmodes are derived from the influence function matrix of the DM. The derivative of the influence function matrix ($\nabla\boldsymbol{\omega}$) can be converted into a multiplication of three matrices by singular value decomposition (SVD):

$$\nabla\boldsymbol{\omega} = (\nabla\mathbf{U})\mathbf{S}\mathbf{V}^{\mathbf{T}}. \tag{8}$$

Matrix **U** is given as

$$\mathbf{U} = \boldsymbol{\omega}(\mathbf{S}\mathbf{V}^{\mathbf{T}})^{-1}. \tag{9}$$

The columns of matrix **U** are called DM eigenmodes, whose orthogonality is the same as Lukosz modes as described in Eq. (2).

Another difficulty of using Eq. (7) is that the calibration of matrix **T** must be done under an aberration-free optical system, which can be difficult to achieve in practice. Furthermore, the linear relationship between **W** and **a** is broken when the aberration is too large or the detector radius R is not properly defined[6].

We will still use the metric function defined by Eq. (6), but the coefficient of each mode is obtained by solving a parabolic equation set and the calibration process can be avoided. For different magnitude aberrations, the mean metric function value is calculated to show the parabolic relationship between the modulus of the error vector and metric function (Fig. 1). The simulated metric function changing curve agrees well with the best-fitting parabola. Here, $\mathbf{a}'$ is the coefficient vector of the DM eigenmodes.

The initial metric function is assumed as J_0. After adding a positive modal bias $+b'_iE_i$ to the optical system by the DM, where b'_i is the modal bias coefficient and E_i is the corresponding DM eigenmode, the metric function

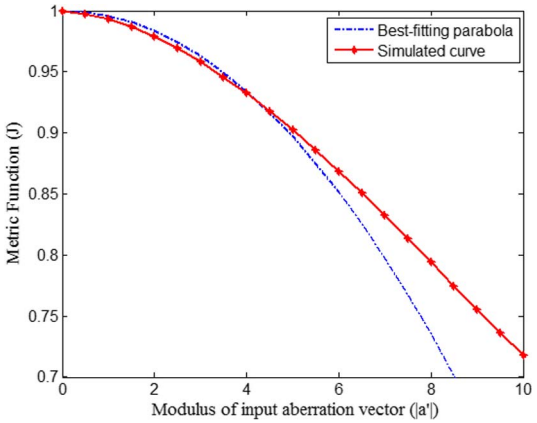

Fig. 1. Parabolic relationship between the input aberration and the metric function.

changes from J_0 to J_+. Similarly, we can get J_- by introducing a negative modal bias $-b'_iE_i$. For each DM eigenmode, a parabolic equation set like Eq. (10) can be obtained. The system's initial aberration is taken into account in Eq. (10), so the calibration process in the traditional method can be avoided:

$$\begin{cases} J_0 = 1 - \frac{\mu}{R^2}\sum_{k\neq i} a'^2_k - \frac{\mu}{R^2}a'^2_i, \\ J_+ = 1 - \frac{\mu}{R^2}\sum_{k\neq i} a'^2_k - \frac{\mu}{R^2}(a'_i + b'_i)^2, \\ J_- = 1 - \frac{\mu}{R^2}\sum_{k\neq i} a'^2_k - \frac{\mu}{R^2}(a'_i - b'_i)^2. \end{cases} \tag{10}$$

Each DM eigenmode coefficient can be solved from Eq. (10) as

$$a'_i = \frac{b'_i(J_+ - J_-)}{2J_+ - 4J_0 + 2J_-}. \tag{11}$$

From Eq. (11), to estimate one certain mode coefficient, at least three measurements of the metric function (i.e., taking three focal-plane images) are required. To estimate the coefficients of N modes, $2N+1$ measurements should be taken. The estimated wavefront aberration is subsequently corrected by the DM based on the phase conjugation principle.

Simulations were made to compare the performance of our method using Eq. (11) and the traditional method using Eq. (7). A 37-channel DM model with a Gaussian-type influence function is simulated and the coupling coefficient is set as 0.2. Wavefront aberrations were simulated by applying random voltages to the DM. One hundred error samples with certain root-mean-square (RMS) values were generated for correction. The mean wavefront correction accuracy changing with the aberration's RMS value is shown in Fig. 2. Here, the correction accuracy is defined as

$$\varepsilon = 1 - \frac{\sigma_{\text{res}}}{\sigma_0}, \tag{12}$$

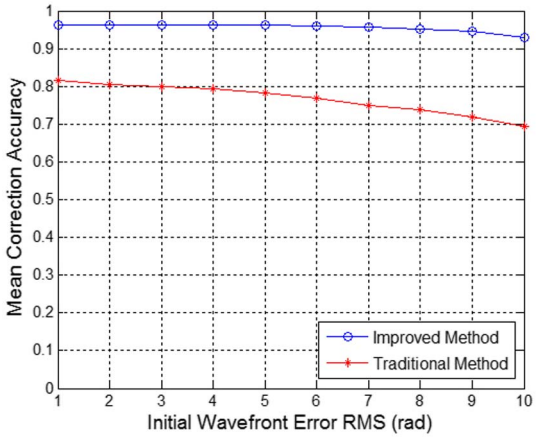

Fig. 2. Mean correction accuracy varied with the wavefront error RMS.

where σ_0 is the RMS of the initial wavefront error and σ_{res} is the RMS of the residual wavefront error. For initial wavefront errors with an RMS of 5 rad, closed-loop correction results of the two methods are presented in Fig. 3. Although both are approaching convergence within three iterations, the residual error of our method is much smaller than the traditional one.

The experimental system layout is illustrated in Fig. 4. The light source is a 635 nm laser coupled with a single-mode fiber. The DM used for both generating and correcting aberrations is a 37-channel micromachined membrane DM from OKO. The influence functions of the DM were measured by a Hartmann–Shack (H-S) wavefront sensor (HASO3 76-GE from Imagine Optics Corporation). The DM eigenmodes were derived from the measured influence function matrix using Eqs. (8)–(9). Then, each DM eigenmode was generated by the DM in sequence and measured by an H-S simultaneously. The fitting error for each mode can be characterized by the RMS difference between the derived modes and the DM-generated modes. The first 10 DM eigenmodes and corresponding fitting errors are shown in Fig. 5. For comparison, the first 10 Lukosz modes

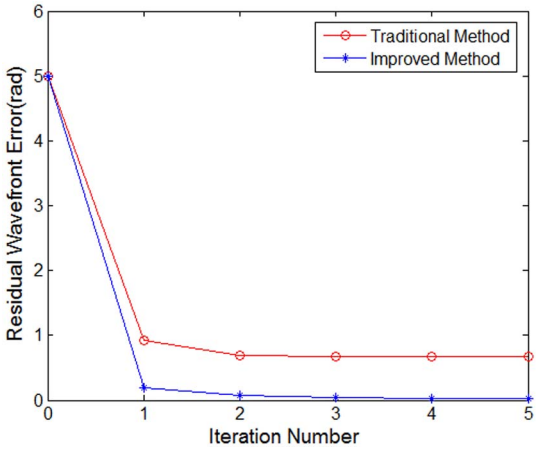

Fig. 3. Residual wavefront error varied with the iteration number.

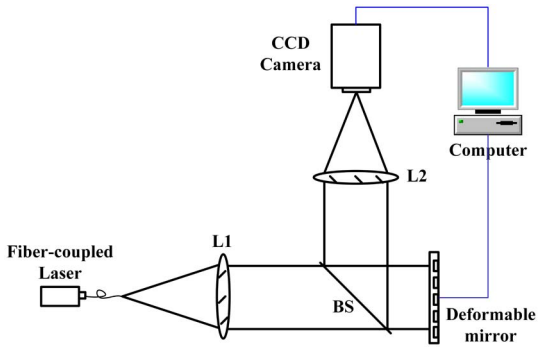

Fig. 4. Experimental system layout.

are also generated by the DM and the fitting errors are given in Fig. 6. Apparently, the fitting error of the DM eigenmodes is negligible and significantly less than that of the Lukosz modes.

An initial distorted focal spot is illustrated in Fig. 7(a). The corrected image using Lukosz modes and Eq. (7) is shown in Fig. 7(b). The corrected image using the DM eigenmodes and Eq. (11) is shown in Fig. 7(c). For both approaches, the first 10 modes as illustrated in Figs. 5 and 6 are used for the correction. Three cycles of correction are performed to ensure the convergence of each method. The initial wavefront aberration and residual wavefront errors were both measured by an H-S sensor; the wavefront RMS value corresponding to each spot is also given in Fig. 7.

In conclusion, we demonstrate an improved model-based WSAO by simulation and experiment. Using DM eigenmodes and solving the parabolic equations directly, the improved method is more feasible and the corrective

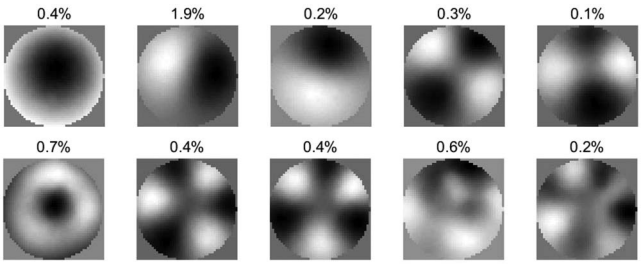

Fig. 5. First 10 DM eigenmodes and the corresponding fitting errors.

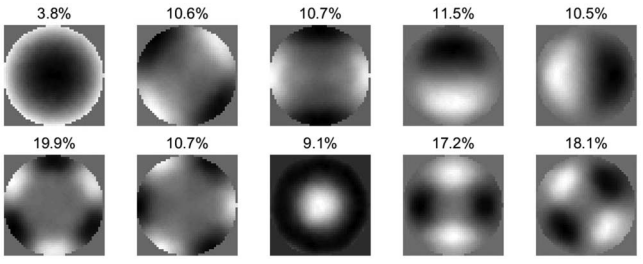

Fig. 6. First 10 Lukosz modes and the corresponding fitting errors.

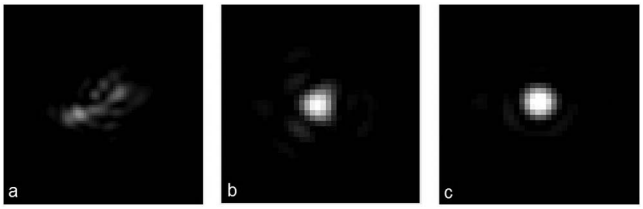

Fig. 7. (a) Initial spot, RMS = 0.34λ; (b) the corrected spot using the traditional method, RMS = 0.084λ; (c) the corrected spot using the improved method, RMS = 0.041λ.

accuracy is also higher than the traditional one. More experiments should be done for continuous or pulsed solid-state lasers to verify the performance of this algorithm in the future.

This work was supported by the National Natural Science Foundation of China (No. 61505008) and the Specialized Research Fund for the Doctoral Program of Higher Education (No. 20131101120023).

References

1. P. H. Merritt and J. R. Albertine, Opt. Eng. **52**, 021005 (2013).
2. P. Yang, Y. Liu, W. Yang, M.-W. Ao, S.-J. Hu, B. Xu, and W.-H. Jiang, Opt. Commun. **278**, 377 (2007).
3. X. Lei, B. Xu, P. Yang, L. Dong, W. Liu, and H. Yan, Chin. Opt. Lett. **10**, 021401 (2012).
4. X. Lei, S. Wang, H. Yan, W. Liu, L. Dong, P. Yang, and B. Xu, Opt. Express **20**, 22143 (2012).
5. M. J. Booth, Opt. Express **14**, 1339 (2006).
6. M. J. Booth, Opt. Lett. **32**, 5 (2007).
7. L. Huang and C. Rao, Opt. Express **19**, 371 (2011).
8. D. Débarre, E. J. Botcherby, T. Watanabe, S. Srinivas, M. J. Booth, and T. Wilson, Opt. Lett. **34**, 2495 (2009).
9. B. Wang and M. J. Booth, Opt. Commun. **282**, 4467 (2009).
10. J. Yu and B. Dong, Acta Opt. Sin. **35**, 0322004 (2015).
11. B. Dong and J. Yu, Chin. Opt. Lett. **13**, 041101 (2015).